01 Jan 2022

# Dielectric Loss Tangent Extraction using Two Single-Ended Striplines of Different Width

Jiangshuai Li

Yuanzhuo Liu

Liang Liu

Shengxuan Xia

*et. al. For a complete list of authors, see https://scholarsmine.mst.edu/ele_comeng_facwork/4678*



## Recommended Citation

J. Li et al., "Dielectric Loss Tangent Extraction using Two Single-Ended Striplines of Different Width," *2022 IEEE International Symposium on Electromagnetic Compatibility and Signal/Power Integrity, EMCSI 2022*, pp. 86 - 91, Institute of Electrical and Electronics Engineers, Jan 2022.
The definitive version is available at https://doi.org/10.1109/EMCSI39492.2022.9889568

# Dielectric Loss Tangent Extraction Using Two Single-ended Striplines of Different Width

Jiangshuai Li[#1], Yuanzhuo Liu[#2], Liang Liu[#3], Shengxuan Xia[#4], Scott Hinaga[+5], Victor Khilkevich[#6]
[#] EMC Laboratory, Missouri University of Science and Technology, Rolla, MO, USA
[+]Cisco Systems, Inc, San Jose, CA. 95134 USA
[1]lijiangs, [2]liuyuanz, [3]llmcr, [4]sx7c3, [6]khilkevichv@mst.edu
[5]shinaga@cisco.com

2022 IEEE International Symposium on Electromagnetic Compatibility & Signal/Power Integrity (EMCSI) | 978-1-6654-0929-2/22/$31.00 ©2022 IEEE | DOI: 10.1109/EMCSI39492.2022.9889568

***Abstract*—Frequency-dependent electrical properties of dielectric materials are one of the most important factors for high-speed signal integrity design. Recently a method of accurately measuring the dielectric loss tangent (tan $\delta$) of differential lines was proposed. By taking into account the ratio between the differential and common mode per-unit-length resistances the surface roughness contribution to the total loss is eliminated and dielectric parameters can be determined. In this article a similar method is applied to a combination of two single-ended lines. To evaluate the accuracy of the extraction, the impact of the de-embedding errors was investigated, which allows to optimize the test PCB design. The extraction method was validated in measurement using a PCB with several two-width pairs of striplines. The extracted loss tangent of several optimal two width pairs of single-ended lines is validated by the SPDR measurements.**

***Keywords —Loss tangent, surface roughness, cross-sectional analysis, S-parameters, de-embedding, error analysis, SPDR.***

## I. Introduction

Adequate wideband characterization of printed circuit board (PCB) dielectric substrates is critical nowadays in high-speed signal and power integrity design. Traditional approximations using frequency-independent dielectric constant ($\varepsilon_r$ also known as DK) and loss tangent ($\tan\delta$ also known as DF) might be applicable for low-speed transmission lines [1-2], however, they do not properly account for the extra attenuation caused by dielectrics polarization at higher frequencies and cannot model phase-delay responses correctly, producing underestimated dielectric loss and noncausality [3]. Inaccurate frequency-dependence will cause significant uncertainty for modern high-speed PCB design, leading to potential failures to meet required specifications or costly overdesign.

A traditional dielectric material properties extraction method using a split post dielectric resonator (SPDR) [4]–[5] is widely adopted by material vendors to provide nominal $\varepsilon_r$ and $\tan\delta$ values at certain frequency. However, the SPDR measurement is an inherently narrow-band method. To cover a certain frequency band, multiple SPDRs are needed. Also, the required dielectric sample cannot contain any metallization layers, which often requires the fabrication of dedicated samples with potentially different properties compared to the multilayer PCB fabrication process [6]. The "Root-Omega" transmission-line-based extraction method [7] was developed to overcome drawback of the SPDR method, but it cannot separate the conductor attenuation factor influence by unknown surface roughness well enough as addressed in [8].

Recently, a new dielectric characterization method using physics-based principles to exclude the influence of foil surface roughness is proposed [9], which offered comprehensive analysis on the extraction procedure based on differential transmission line model. Based on the method introduced in [8] , in this paper we propose a similar extraction method using, however two single-ended transmission lines with different trace width instead of a differential pair. Single-ended measurements are usually simpler than that the differential one which make the single-ended extraction method more appealing in practice.

This article is arranged as follows. In section II, the core algorithm of the two-width single-ended lines extraction model is introduced. In section III, the extraction model is validated in simulation, and we further investigate the influence of the de-embedding error on the performance of the extraction model. Section IV implements the extraction model in measurement using several two width pairs of single-ended lines. Finally, the summary is given.

## II. Loss Tangent Extraction Methodology

Let us assume two single-ended transmission lines. Shown in Fig. 1, these two single-ended lines are marked by subscript 1 and 2, and have different conductor width $w_1$ and $w_2$. The propagation constant for each line is related to the PUL parameters as

$$\gamma_{1,2} = \sqrt{(R_{1,2} + j\omega L_{1,2})(G_{1,2} + j\omega C_{1,2})}, \quad (1)$$

$$\gamma_{1,2} = \alpha_{1,2} + j\omega\beta_{1,2}\,. \quad (2)$$

where $\alpha$ is the attenuation factor and $\beta$ is the phase constant. In practical low-loss transmission lines ($R \ll \omega L$ and $G \ll \omega C$), the attenuation factor can be approximately calculated as

$$\alpha \approx \frac{1}{2}\left(R\sqrt{\frac{C}{L}} + G\sqrt{\frac{L}{C}}\right). \quad (3)$$

The dielectric loss is characterized by the conductance $G$ [1], therefore, the extraction of the $\tan\delta$ requires the determinations of all other PUL parameters (R, L, and C) and the attenuation factor in (3).

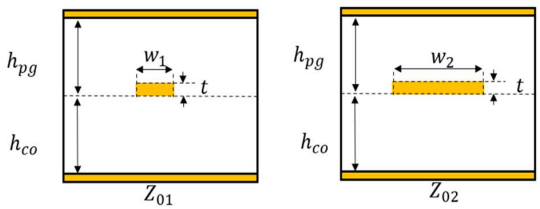


Fig. 1. Cross-section of two single-ended striplines.

The attenuation factor can be determined in the insertion loss measurement of the target single-ended traces as

$$\alpha = \frac{-\ln(|S_{21}|)}{l}. \tag{4}$$

where $S_{21}$ is the de-embedded (i.e. the transitions are removed and the $S_{21}$ is normalized to the actual impedance of the line) insertion loss and $l$ is the length of the transmission line after de-embedding.

The PUL capacitances and inductances can be determined in Q2D (a 2-D cross-sectional solver) simulation for a known geometry and the dielectric permittivity of the transmission line. In [9] it has been derived and illustrated that the relative permittivity factor of the trace can be calculated by

$$\varepsilon_r = \frac{1}{\omega^2 \cdot \varepsilon_0 \cdot \mu_0} \cdot \frac{\beta^2 \left(L - \frac{R}{\omega}\right)}{L}. \tag{5}$$

where $L$ and $R$ are calculated in a 2D solver (assuming vacuum medium and no surface roughness), and $\beta$ is calculated based on the de-embedded transmission coefficient measurement as

$$\beta = \left|\frac{\arg(S_{21})}{l}\right|. \tag{6}$$

The PUL capacitance in a stripline is proportional to the permittivity of the dielectric, therefore, with the relative permittivity obtained in (5), the PUL capacitance of the target trace can be calculated as

$$C = C_{vacuum} \cdot \varepsilon_r \tag{7}$$

where $C_{vacuum}$ is obtained in the 2D solver.

Therefore, the PUL inductance $L$ and capacitance $C$ in (3) can be easily obtained from the geometry information and transmission coefficient measurement. However, it is hard to determine the PUL resistance $R$ accurately because of the effect of the surface roughness. In [9] an efficient and straightforward approach to quantify the PUL resistance was proposed by introducing a coefficient $K$ which is defined as the ratio of the modal PUL resistances

$$K = \frac{R_{differential}}{R_{common}}. \tag{8}$$

The same idea can be generalized in the sense that the parameters of any two TL modes propagating in the same dielectric medium can be used to perform the loss tangent extraction. In this paper we will use the modes propagating in two single-ended lines of different width as

$$K = \frac{R_1}{R_2} \tag{9}$$

The PUL conductance $G$ is related to the dielectric loss tangent as

$$G = \omega \cdot C \cdot \tan\delta\,. \tag{10}$$

By combining (3), (8), and (9), the following system of equations can be written [9] as

$$\begin{cases} \alpha_1 = \frac{1}{2}\left(R_1\sqrt{\frac{C_1}{L_1}} + G_1\sqrt{\frac{L_1}{C_1}}\right) \\ \alpha_2 = \frac{1}{2}\left(R_2\sqrt{\frac{C_2}{L_2}} + G_2\sqrt{\frac{L_2}{C_2}}\right) \\ G_1 = \omega \cdot C_1 \cdot \tan\delta \\ G_2 = \omega \cdot C_2 \cdot \tan\delta \\ K = \frac{R_1}{R_2} \end{cases}. \tag{11}$$

By solving (10) with respect to $\tan\delta$, the following expression can be obtained:

$$\tan\delta = \frac{2}{\omega} \frac{\alpha_1\sqrt{\frac{C_2}{L_2}} - \alpha_2\sqrt{\frac{C_1}{L_1}} \cdot K}{\sqrt{\frac{C_2}{L_2}} \cdot \sqrt{C_1 L_1} - \sqrt{\frac{C_1}{L_1}} \cdot \sqrt{C_2 L_2} \cdot K}. \tag{12}$$

This formula relates the attenuation factors, PUL capacitances $C$ and inductances $L$, and the resistance ratio $K$ to the dielectric loss tangent.

The entire dielectric loss tangent extraction procedure is illustrated in the flow chart shown in Fig. 2.

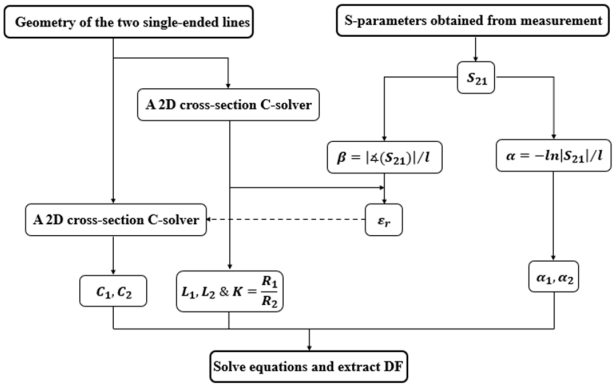


Fig. 2. Flow chart of the proposed loss tangent extraction method.

## III. Simulation Validation and Error Analysis for the Loss Tangent Extraction Method

To illustrate the feasibility of the proposed method, it is first applied to simulated transmission lines.

### *A. A. Accuracy of Extracted Loss Tangent in Simulation.*

Shown in Fig. 3, 2-D models of two single-ended striplines with different trace width were created. Using Ansys Q2D to solve the 2-D cross-sectional problem, the necessary PUL parameters as well as the transmission coefficients of the two lines were calculated. The permittivity value is extracted by using (5) and (6). Finally, the loss tangent is calculated by (12) and compared to the actual value.

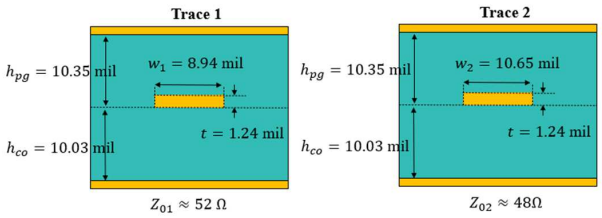


Fig. 3. Cross-section of two single-ended transmission lines of different conductor width used for loss tangent extraction.

To illustrate the extraction accuracy, the model shown in Fig. 3 was filled with the uniform dielectric material with the slightly dispersive dielectric modeled according to Djordjevic with $\varepsilon_r = 3.54$ and $\tan\delta = 0.0066$ at 1 GHz.

Fig. 4 shows the extracted values of the permittivity and loss tangent along with the actual values that we set in the Q2D model. As can be seen in Fig. 4(a), the extracted permittivity curve practically overlaps with the actual one (the error does not exceed 0.5%), which validates the permittivity extraction method in (5) and (6). In Fig. 4(b-c), the loss tangent extracted by (12) matches the actual curve very well in the almost entire frequency range; however below 0.5 GHz, the extracted loss tangent deviates more significantly from the actual value. Nevertheless, the extraction error never exceeds 5% and in much better at higher frequencies (Fig. 4 (c)).

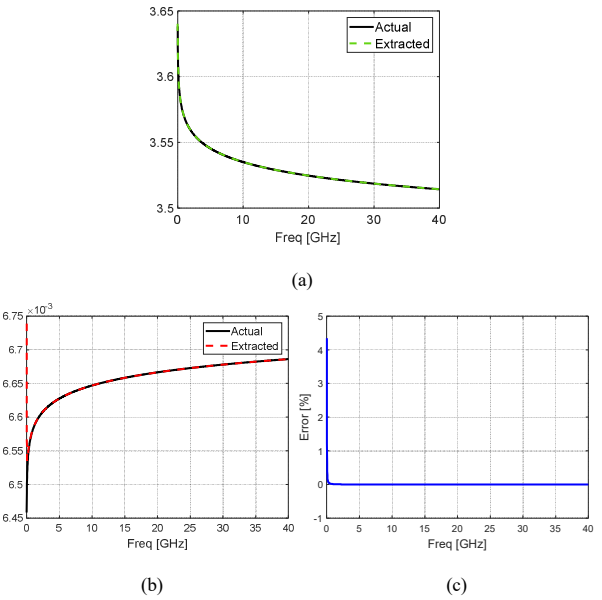


Fig. 4. Extracted dielectric permittivity (a) and loss tangent (b): (a) extracted permittivity the error of extracted loss tangent (c).

*B. De-embedding error analysis.*

The validation in the previous section assumed no errors in the input parameters, which is impossible on practice. This section provides the analysis of de-embedding errors on the extraction accuracy[10]-[11].

The proposed loss tangent extraction model requires several groups of data:

(1) raw S-parameters obtained in the VNA measurement;
(2) de-embedded S-parameters to obtain attenuation factors;
(3) PUL inductance, capacitance, and resistance ratio $K$ calculated by a 2-D cross-sectional solver.

Therefore, three sources of errors can be identified: measurement errors, de-embedding errors, and simulation errors. As has been addressed in [9], not all of these errors can be estimated accurately. Among these three kinds of error, the simulation errors are especially difficult to determine directly because the actual PUL parameters of the lines are not accessible; the VNA measurement errors strongly depend on the VNA model, calibration technique, quality of cables and connectors and is very difficult to assess in general terms. Therefore, this work mainly concentrated on the de-embedding error analysis since it has obvious effects on the loss tangent extraction model with a relatively large error contribution. Even if other types of errors are not quantified, the de-embedding errors analysis is still useful because it allows optimization of the extraction PCB design.

Any suitable de-embedding procedure can be used to obtain the transmission coefficient. In the present implementation, a variant of the 2x-thru de-embedding technique known as "eigenvalue de-embedding" [9] was used. The choice was made primarily because it is a precise de-embedding technique for translationally uniform transmission lines and uses a minimal number of standards (just two lines of different length).

All de-embedding methods require identical fixtures in total and thru lines (for trace 1: Fixture 1 = Fixture 1′, Fixture 2= Fixture 2′, as shown in Fig. 5). For the "eigenvalue" de-embedding (also known as "Delta-L") [Eigenvalue de-embedding] method used in this study, the symmetric design in fixtures for both total and thru lines is also required such that all four fixtures are identical.

As analyzed in [9] the transitions from coaxial to strip-line medium cannot be made perfectly identical due to geometrical variations and variability in the connector-pad transitions. For the sake of the error analysis, we assume that the source of de-embedding inaccuracies is the variations in the transitions from the coaxial cable to the single-ended lines [12]-[13], violating identical and symmetrical assumptions formulated above.

The coaxial stripline discontinuities are modelled with the excessive capacitance and inductance as shown in Fig. 6. The values of excessive capacitance and inductance are assumed to be normally distributed random variables. The expected values and standard deviations from [8] were used for the de-embedding error modeling: $\mu_L = 17.5\,pH$, $\sigma_L = 40\%$, $\mu_c = 48\,fF$, $\sigma_c = 11\%$. Since the lines of two different widths are used for each measurement and each width line has two lines of different length for de-embedding purposes, a total of eight fixture models are created as shown in Fig. 6(b). All capacitances and inductances in the modes are treated as independent random variables.

After the fixture and single-ended lines model are created, 200 combinations of total and thru S-parameters are created for de-embedding. The actual dielectric parameters in the modes were set as $\varepsilon_r = 4$ and $\tan\delta = 0.005$ at 10 GHz. The widths of the traces are treated ad two independent variables. An example of the loss tangent extraction for $w_1 = 5$ mil and $w_2 = 50$ mil is shown in Fig. 7(a). The plot contains 200 curves corresponding to different (random) values of the fixture excessive reactances. The standard deviation $\sigma_{DF}$ is then calculated to quantify the performance of the loss tangent extraction method as shown in Fig. 7(b).

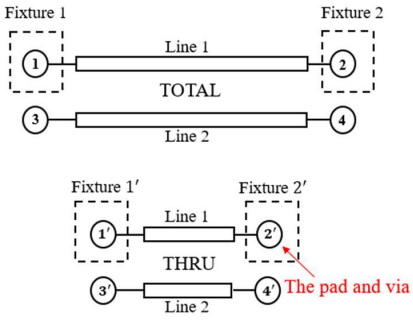


Fig. 5. Total and Thru fixture definition.

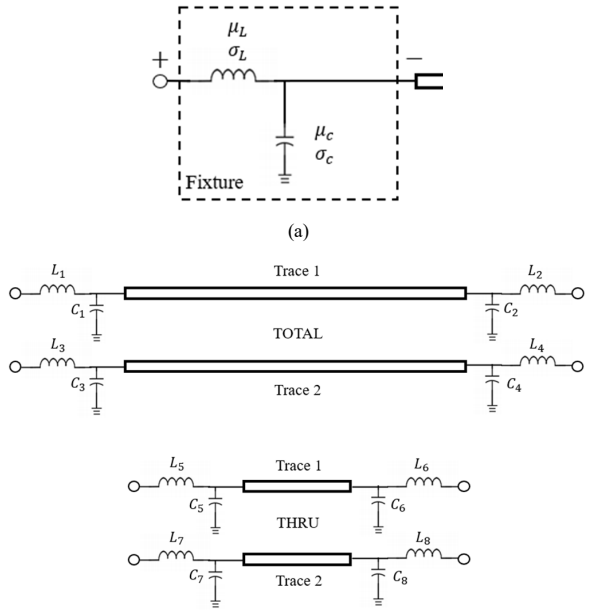


(a)

(b)

Fig. 6. Circuit model of the fixture (a) and total de-embedding pattern model (b).

As can be seen from the plot, the standard deviation of extracted loss tangent, in general, increases with frequency due to the increase of the fixture reflections (and hence increased influence of their variability); however, at some frequencies where the de-embedding equation is relatively poorly conditioned, the sensitivity to errors is higher. In general, the error curve contains a periodic pattern, the periodicity of which depends on the electrical lengths of the thru and total standards.

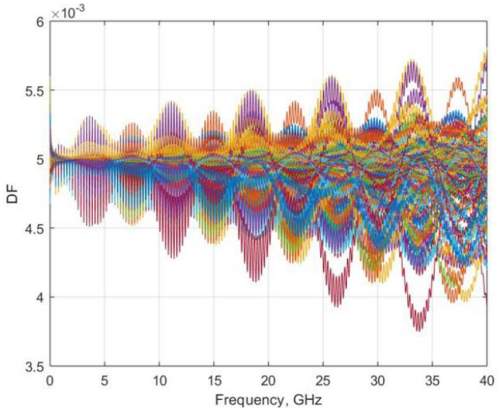


(a)

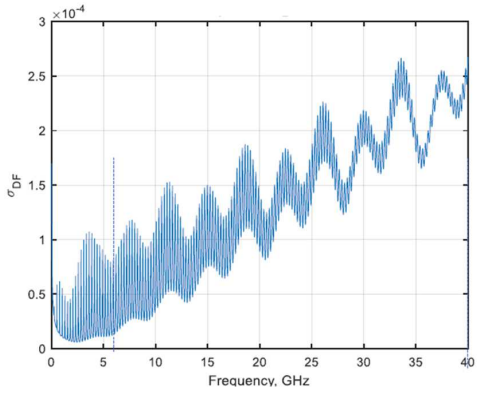


(b)

Fig. 7. Extracted loss tangent curves from the 200 trials (a) and the standard deviation of the extracted loss tangent results(b).

It is obvious that low values of the extracted loss tangent variations are preferable. To find the optimum pair of trace widths, the maximum value of the extracted loss tangent standard deviation in the frequency range of 6 GHz to 40 GHz was plotted. To do so the widths were swept from 5 mil to 100 mil with a 5-mil step. The de-embedding error analysis is applied to each width combination as described above with the exception of those pairs of equal width ($w_1 \neq w_2$) for which the de-embedding cannot be performed.

The trace width sweeping result is shown in Fig. 8. The ratio of maximum $\sigma_{DF}$ to the mean value of the loss tangent is calculated and plotted in the dB scale as the color axis. In Fig. 8, the blue regions indicate the width pairs with the lowest extraction errors. The plot shows that the de-embedding error generally decreases as the difference between the trace width increases, at the same time when the width becomes too small or extreme large the error increases as well because impedance mismatch between the line and the ports. The optimal trace width pairs occur in the region indicated by the ellipse. By analyzing the line impedance as a function of the trace width (Fig. 9) it can be concluded that the optimum combinations include one line with the impedance close to the impedance of the ports (10 mil trace) and another line with the impedance between 1/2 to 1/5 of the port impedance.

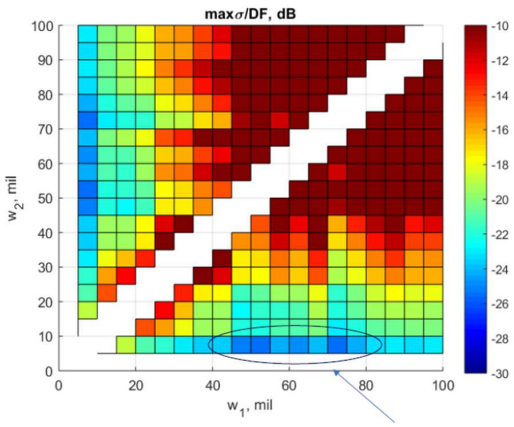


Fig. 8. Maximum normalized standard deviation of the extracted loss tangent as a function of the trace width.

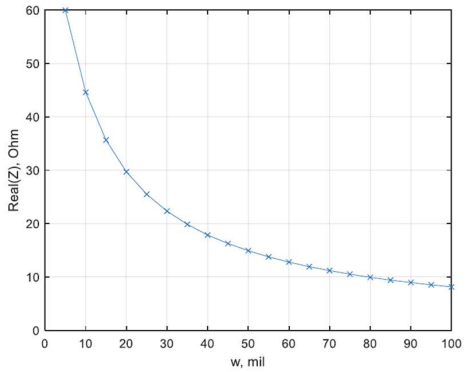


Fig. 9. The impedance of the single-ended line as a function of the width.

## IV. Loss Tangent Extraction Using Measurement Data

To test the proposed method in the experiment, a test vehicle containing multiple single-ended lines was fabricated. The layout plan view of the PCB is shown in Fig. 10 (a): a total of 8 single-ended line pairs are created (the widths are 200 mil, 100 mil, 50 mil, 30 mil, 20 mil, 10 mil, 7.5 mil, and 5 mil); each pair has a "total" line (5 inch) and a "2xthru" line (1 inch) for the de-embedding process.

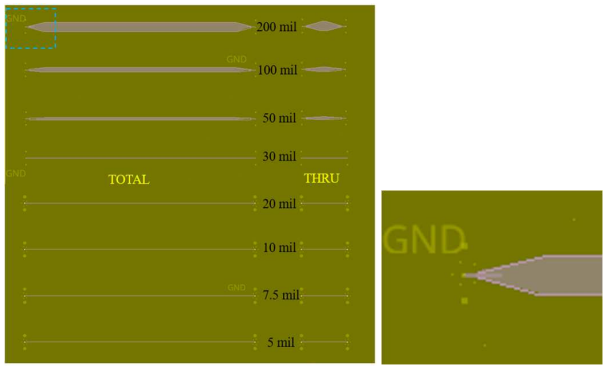


| Layer | Material Type | Thickness | |
|---|---|---|---|
| Top Layer1 | Copper | 0.035 mm | |
| Prepreg | 7628*1 | 0.2 mm | |
| Inner Layer2 | Copper | 0.0175 mm | 0.3 mm (with copper core) |
| Core | Core | 0.265 mm | |
| Inner Layer3 | Copper | 0.0175 mm | |
| Prepreg | 7628*1 | 0.2 mm | |
| Bottom Layer4 | Copper | 0.035 mm | |

(a)

(b)

Fig. 10. Layout and stack-up information (a) and the photograph of the board showing the SPDR sample region (b).

To reduce the reflections at the transitions, the traces were tapered at the ends. A portion of the PCB was left without metallization in the ground plane layers to serve as a pure-dielectric sample for the SPDR measurement, shown in Fig. 10(b) the yellow region at the corner of the PCB. The SPDR measurements were performed at three discrete frequencies. The results are summarized in Table 1.

Table. 1. Reference permittivity and loss tangent values extracted by SPDR method.

| Freq [GHz] | 10 | 15 | 20 |
|---|---|---|---|
| Loss Tangent | 0.0147 | 0.0157 | 0.0160 |
| Permittivity | 4.61 | 4.58 | 4.54 |

To quantify the extracted loss tangent accuracy the SPDR values are used as the reference. The SPDR values are interpolated on the frequency range from 10 GHz to 20 GHz and the mean square error is calculated as

$$MSE_{DF} = \frac{1}{m}\sum_{i=1}^{m}\left(\frac{\tan\delta_S(i) - \tan\delta_t(i)}{\tan\delta_S(i)}\right)^2, \qquad (13)$$

where $\tan\delta_S$ is the SPDR extraction result, $\tan\delta_t(i)$ is the two-width extraction result, and $m$ is the number of frequency samples between 10 GHz and 20 GHz.

The resulting MSE value is shown in Fig. 11 in the dB scale. As can be seen from the figure the obtained MSE pattern is in generally similar to that in Fig. 8 which validates the proposed de-embedding model. The relatively low MSE pairs were: 5 mil/20 mil, 5 mil/50 mil, 5 mil/100 mil, 10 mil/100 mil which agrees with the conclusion in the previous section.

The extracted loss tangent curves of the pairs with the lower MSE values are shown in Fig. 12. The black curve is the SPDR extracted loss tangent after interpolation. As can be seen the loss tangent curves extracted by the two-width method match the SPDR result well. At low frequencies (<5 GHz) the extraction accuracy suffers similarly to the results reported in [8]. This can be explained by the measurement and simulation errors which have larger weight at lower frequencies (Fig. 24 in [8]). However, from 5 GHz to 30 GHz, the loss tangent curves are relatively stable and smooth.

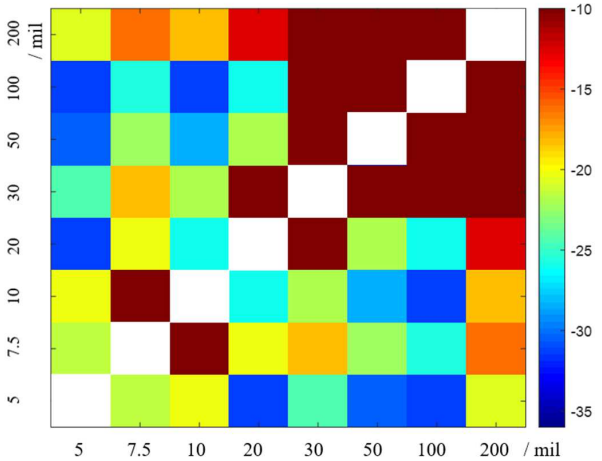


Fig. 11. MSE (dB) of loss tangent extracted from all available two-width pairs.

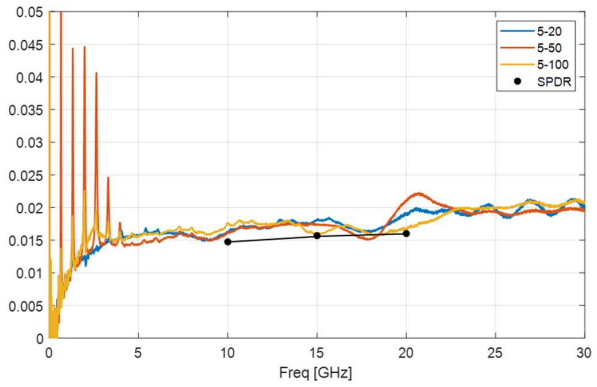


Fig. 12. Extracted loss tangent curves for the best width pairs.

## V. SUMMARY

A new loss tangent extraction method is proposed and analyzed. The method uses two single-ended lines of different trace width to implement the loss tangent extraction based on transmission line cross-sectional information and measured transmission coefficient. To estimate the accuracy of the extraction, the influence of the de-embedding errors is analyzed. The analysis allows determination of the optimal width combination. The two-width extraction model was validated with physical measurements using a specially designed PCB. The extracted loss tangent of selected width pairs matches well with the reference SPDR data.

## ACKNOWLEDGMENT

This material is based upon work supported by the National Science Foundation (NSF) under Grant No. IIP-1916535.

## REFERENCES

[1] Y. Guo, D. Kim, J. He, S,. Yong, Y. Liu, B. Pu, X. Ye, J. Fan ., "The Simulated TDR Impedance In PCB Material Characterization," *2021 IEEE International Joint EMC/SI/PI and EMC Europe Symposium*, 2021, pp. 831-834.

[2] Y. Liu, S. Yong, J. Li and V. Khilkevich, "Dielectric Constant Extraction for Microstrip Transmission Lines Based on S-parameter Measurements and Cross-section", 2021 IEEE International Joint EMC/SI/PI and EMC Europe Symposium, 2021, pp.982-987.

[3] S. Yong, Y. Liu, et al., "Dielectric Dissipation Factor (DF) Extraction Based on Differential Measurements and 2-D Cross-sectional Analysis," 2018 IEEE Symposium on Electromagnetic Compatibility, Signal Integrity and Power Integrity (EMC, SI & PI), Long Beach, CA, 2018, pp. 217-222.

[4] J. Krupka and S. Maj, "Application of the $TE_{01}$ mode dielectric resonator for the complex permittivity measurements of semiconductors", *Proceedings of CPEM '86*, pp. 154-155, 1986.

[5] J. Krupka, R.G. Geyer, J. Baker-Jarvis, and J. Ceremuga, "Measurements of the complex permittivity of microwave circuit board substrates using split dielectric resonator and reentrant cavity techniques", Proceedings of DMMA'96 Conf., Bath, U.K., 23-26 Sept. pp. 21-24, 1996.

[6] J. Krupka, A P Gregory, O C Rochard, R N Clarke, B Riddle and J Baker-Jarvis, "Uncertainty of Complex Permittivity Measurements by Split-Post Dielectric Resonator Technique", Journal of the European Ceramic Society, vol. 21, pp. 2673-2676, 2001.

[7] X. Tian et al., "Numerical investigation of glass-weave effects on highspeed interconnects in printed circuit board," in Proc. IEEE Int. Symp. Electromagn. Compat., 2014, pp. 475–479.

[8] S. Jin, B. Chen, X. Fang, H. Gao, and J. Fan, "Improved 'root-omega' method for transmission-line based material property extraction for multilayer PCBs," IEEE Trans. Electromagn. Compat., vol. 59, no. 4, pp. 1356–1367, Mar. 2017.

[9] S. Yong *et al*., "Dielectric Loss Tangent Extraction Using Modal Measurements and 2-D Cross-Sectional Analysis for Multilayer PCBs,"in *IEEE Transactions on Electromagnetic Compatibility*, vol. 62, no. 4, pp. 1278-1292, Aug. 2020.

[10] Y. Liu et al., "S-Parameter De-Embedding Error Estimation Based on the Statistical Circuit Models of Fixtures," *in IEEE Transactions on Electromagnetic Compatibility*, vol. 62, no. 4, pp. 1459-1467, Aug. 2020.

[11] S. Yong, Y. Liu, et al., "A Practical De-embedding Error Analysis Method Based on Statistical Circuit Models of Fixtures," *2019 IEEE International Symposium on Electromagnetic Compatibility, Signal & Power Integrity (EMC+SIPI)*, New Orleans, LA, USA, 2019, pp. 45-50.

[12] B. Chen, X. Ye, B. Samaras, and J. Fan, "A novel de-embedding method suitable for transmission-line measurement," in *Proc. IEEE Asia-Pac.* Symp. Electromagn. Compat., 2015, pp. 1–4.

[13] Q. Huang, J. Li, J. Zhou,W.Wu,Y.Qi, and J. Fan, "De-embedding method to accurately measure high-frequency impedance of an O-shape spring contact," in Proc. Int. Symp. IEEE Electromagn. Compat., 2014, pp. 600–603.